Formation and properties of the nanocluster structure of iron oxides

I. P. Suzdalev,[a] Yu. V. Maksimov,[a] V. K. Imshennik,[a] S. V. Novichikhin,[a] V. V. Matveev,[a] Yu. D. Tret´yakov,[b] A. V. Lukashin,[b] A. A. Eliseev,[b] N. V. Avramenko,[c] A. A. Malygin,[d] and E. A. Sosnov[d]*

[a]*N. N. Semenov Institute of Chemical Physics, Russian Academy of Sciences, 4 ul. Kosygina, 119991 Moscow, Russian Federation. Fax: +7 (495) 137 8318. E-mail: suzdalev@chph.ras.ru*
[b]*Department of Materials Science, M. V. Lomonosov Moscow State University, 1 Leninskie Gory, 119992 Moscow, Russian Federation. Fax: +7 (495) 939 0998. E-mail: lukashin@inorg.chem.msu.ru*
[c]*Department of Chemistry, M. V. Lomonosov Moscow State University, 1 Leninskie Gory, 119992 Moscow, Russian Federation. Fax: +7 (495) 932 8846. E-mail: natali@td.chem.msu.ru*
[d]*St. Petersburg State Institute of Technology (Technical University), 26 Moskovsky prosp., 190013 St. Petersburg, Russian Federation. Fax: +7 (812) 259 4886. E-mail: malygin@lti-gti.ru*

Nanostructures based on iron oxide clusters 1—300 nm in size were synthesized and studied. Thermodynamic models of nanocluster nucleation resulting in the formation of both primary nanoclusters and nanocluster aggregates with the sizes up to 70—80 nm were considered. Models of heat capacity of the nanoclusters were examined, and the twofold increase in the heat capacity of the iron oxide clusters 2—3 nm in size compared to that of the bulk iron oxide samples was found. The size of the primary nanoclusters and the intercluster interaction make it possible to vary the magnetic properties of the nanostructures in a wide range from paramagnetic to magnetically ordered α-Fe_2O_3—γ-Fe_2O_3 nanostructures with the first-order magnetic phase transitions, magnetic twinning, and a strong magnetic field (10 Oe) effect on the magnetization increase at low temperatures.

Key words: nanoclusters and nanostructures, nanocluster design, heat capacity, magnetic phase transitions, magnetization, Mössbauer spectroscopy, atomic force microscopy.

Nucleation and formation of nanoclusters from the gas phase, solutions, and melts are known and well studied processes characterized by critical nucleation sizes.[1,2] Processes of cluster nucleation in the solid phase are much more complicated and less controllable. In this case, topochemical reactions leading to the appearance of a new phase can be used. For homogeneous nucleation, the minimum cluster size is determined by the critical nucleation radius, and the maximum radius is determined by diffusion restraint of mobility of components of the new phase formed due to the topochemical reaction.[3] In the case of matrix or template restraint, the minimum and maximum cluster sizes are determined by the nanoreactor sizes.[4] The further growth of clusters, for instance, with the temperature increase, can result in cluster agglomeration; in this case, the initial weak intercluster interaction characteristic of the minimum critical cluster sizes is replaced by the strong intercluster interaction.[5] Solid-phase nucleation also occurs when nanocrystallites are formed from the amorphous phase (metals and alloys, amorphous polymers) upon detonation processes, explosions, *etc.*[6]

The formation of nanoclusters and a solid-phase nanostructure is very complicated; however, these are the processes that determine the final properties of such nanomaterials as metal alloys, ceramics, glasses, and organic polymers. Therefore, it is significant to develop models of nucleation interpreting the change or control of the properties of nanostructures. The model of homogeneous nucleation and agglomeration of iron oxide nanoclusters upon the thermal decomposition of iron oxalate was proposed.[3,5] It was shown that both weakly interacting, virtually separated with the media iron oxide nanoclusters and iron oxide nanoclusters of the initial agglomeration stage are stabilized under certain conditions. This reaction makes it possible to obtain a wide range of iron oxide nanoclusters with the size from one to several hundreds of nanometers and different intercluster interactions and supercluster structures. This, in turn, should result in a wide variation of the properties of nanoclusters. Homogeneous nucleation is the simplest case of cluster formation of iron and oxygen atoms. However, such an atomic nucleation should be accompanied

Published in Russian in *Izvestiya Akademii Nauk. Seriya Khimicheskaya,* No. 10, pp. 1693—1704, October, 2006.
1066-5285/06/5510-1755

by the participation of individual clusters as a whole to form aggregates of clusters.

The purpose of the present work is to synthesize different nanostructures based on iron oxides in a wide range of nanocluster sizes (from several nanometers to several hundreds of nanometers) with a change in the intercluster interactions and, on this basis, variation of their microscopic and macroscopic properties.

Iron(III) oxalate was used as the solid-phase medium of formation and growth of the iron oxide nanoclusters.

Experimental

Iron oxide nanoclusters were prepared by the thermal decomposition of iron(III) oxalate $Fe_2(C_2O_4)_3 \cdot 5H_2O$ in air at 200—350 and 500 °C.[3]

The microstructure of the sample surface was studied on a Solver P47 Pro scanning probe microscope with an AFM (atomic force microscopy) scanning head in the semicontact regime in air using a silicon cantilever (probe radius 10 nm). Powders under study were molded under a pressure of 110 bar in the reach-through hole of a nickel plate followed by the removal of excess material. The nickel support was placed on a dielectric corundum plate, the sample was scanned over several regions, and the most characteristic features of its structure were studied.

Heat capacity was measured on a Mettler DSC-30 differential scanning calorimeter in a nitrogen flow in the temperature interval from 110 to 300 K with a scan rate of 3—5 deg min^{-1}.

Magnetic measurements were carried out on a Criogenics SQUID S-600 magnetometer with cooling in the zero field (ZFC) and in a magnetic field of 10 Oe (FC). To provide the ZFC regime, a sample was cooled to 1 K in the absence of an external magnetic field, and then measurements were carried out in a field of 20 Oe, increasing temperature to 300 K with an increment of 1—20 K. For measurements in the FC mode, the sample was cooled to 1 K in an external magnetic field of 10 Oe, after which measurements were conducted in a field of 20 Oe, increasing temperature to 300 K with an increment of 1—20 K.

Mössbauer spectra were obtained on a Wissel spectrometer with the ^{57}Co (Rh) γ-radiation source with an activity of 10 mCi. Isomeric shifts were calculated from the center of the spectrum of the magnetic hyperfine structure (HFS) of metallic iron.

Results and Discussion

Thermodynamic models of atomic and cluster nucleation in the solid phase. During the thermal decomposition of iron(III) oxalate, a mobile active reaction medium begins to form with nucleation of iron oxide nanoclusters at a temperature higher than the critical point. Cluster formation is similar to nucleation from individual atoms in solution or melt in a restricted volume (volume of a cell or pore). This size is controlled by diffusion restraint that does not allow perturbation of the mother medium, which is caused by a change in the cluster size, to migrate farther than at the distance $L \approx (Dt)^{1/2}$ (D is the diffusion coefficient) during the nucleation time (t). In this case, this size can be considered as the size of a cell surrounding the cluster beyond which components of the mother batch cannot penetrate.

For a system of non-contacting clusters, the dependence of the free Gibbs energy (ΔG_{fc}) on the cluster radius (r) for one cluster during atomic nucleation is determined by the formula

$$\Delta G_{fc} = 4\pi r^2 \alpha_c - (4/3)\pi r^3 \rho_c \Delta\mu_c, \quad (1)$$

where ρ_c is the density of iron atoms in the cluster, $\Delta\mu_c$ is the change in the chemical potential of iron on going of one iron atom from the mother batch into the structure of one cluster, and α_c is the density of the free surface energy of the cluster. If N atoms fall on one cluster in a mixture of which n_0 are iron atoms and $n_c = (4/3)\pi r^3 \rho_c$ are iron atoms present in the cluster structure, then for $N \gg n_0$

$$\Delta\mu_c = \Delta\mu_c^0 + \ln[(n_0 - n)/N]. \quad (2)$$

Here $\Delta\mu_c^0$ is the change in the standard chemical potential of iron measured in the kT units on going of one iron atom into the cluster structure. The clusters do not contact with each other at the initial stage. When designating the volume and surface area of this cluster as $V_{fc} = (4/3)\pi r^3$ and $S_{fc} = 4\pi r^2$, respectively, then Eq. (1) can be written in the form

$$\Delta G_{fc} = \alpha S_{fc} - \{\Delta\mu_c^0 + \ln[(n_0 - n)/N]\} V_{fc}. \quad (3)$$

The $\Delta G_{fc}/\Delta G_{cr}$ function has a maximum in the point $r = r_{cr}$ and a minimum in the point $r = r_{max}$ (Fig. 1).

Equation (3) characterizes the stages of cluster nucleation and growth in a weakly interacting system of noncontacting clusters. The further increase in their sizes results in the situation when they come in contact with each other and begin to agglomerate. The onset of cluster agglomeration characterizes a system of strongly interacting clusters. If the distance between the cluster centers

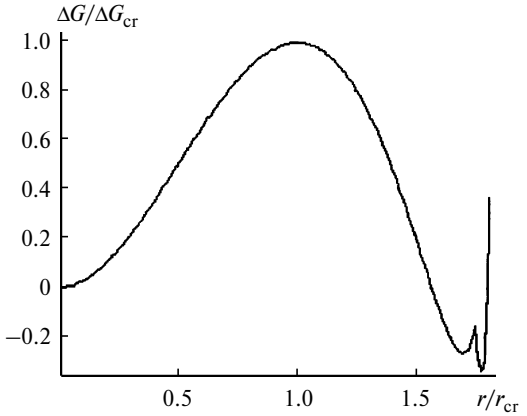

Fig. 1. Change in the free Gibbs energy $\Delta G/\Delta G_{cr}$ upon cluster nucleation, growth, and agglomeration calculated by formulas (3) and (4) as a function of the relative cluster size r/r_{cr}.

is $2r_t$ = const (r_t is the radius of clusters contacting with each other), then the surface area S_{sc} and volume V_{sc} of the cluster forming contacts with k neighbors are determined rather correctly by the expressions

$$S_{sc} = 4\pi r^2 + k2\pi r(r_t - r), \quad (4)$$

$$V_{sc} = (4/3)\pi r^3 + k(1/3)\pi r(-2r^3 + 3r^2 r_t - r_t).$$

Therefore, the change in the free Gibbs energy at the agglomeration stage (*i.e.*, for $r > r_t$) is the following:

$$\Delta G_{sc} = \alpha S_{sc} - \{\Delta\mu^0 + \ln[(n_0 - n)/N]\}\rho V_{sc}. \quad (5)$$

Thus, the profile of changing the free energy of the system per cluster in the whole range of changes is determined for $r < r_t$ by formula (3), and for $r > r_t$ it is determined by formula (5). The plot of $\Delta G/\Delta G_{cr}$ *vs.* r/r_{cr} for $r_t = 1.75R_{cr}$ is shown in Fig. 1 as an example. The plot has three minima separated by two maxima. The minimum in the point $r = 0$ corresponds to the initial state of the mother medium. After passing through r_{cr}, the system transforms into the first stable state ($r = r_{max}$) corresponding to the equilibrium state of the formed but not contacting clusters (this is possible when $r_{max} < r_t$). The third minimum corresponds to a system of agglomerating clusters each of which has k contacts. Therefore, the first maximum at $r = r_{cr}$ forms a potential nucleation barrier, and the second one forms the potential agglomeration barrier. The potential agglomeration barrier for $k = 6$ and different R_t values is presented in Fig. 2. At $r_t = 1.7r_{cr}$ agglomeration is barrierless, whereas at $r_t = 1.75r_{cr}$, *i.e.*, in a system less densely occupied by clusters, a potential barrier should be surmounted to begin agglomeration. In a less denser system, at $r_t = 1.8r_{cr}$, no agglomeration occurs because this is conjugated with an increase in the free energy.

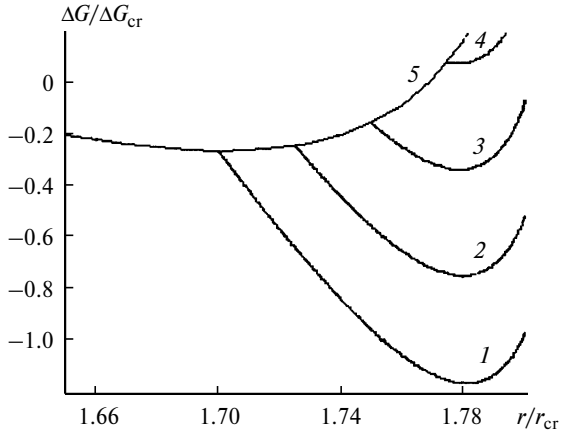

Fig. 2. Changes in the free Gibbs energy $\Delta G/\Delta G_{cr}$ in the region of onset of cluster agglomeration as a function of the relative cluster size r/r_{cr} calculated for different values of the half-distance between the cluster centers: $r_t = 1.70r_{cr}$ (*1*), $1.73r_{cr}$ (*2*), $1.75r_{cr}$ (*3*), $1.77r_{cr}$ (*4*), and $1.80r_{cr}$ (*5*).

Two minima in the curves of differential thermal and gravimetric analysis were found[7] during the thermal decomposition of iron oxalate $Fe_2(C_2O_4)_3 \cdot 5H_2O$ in air at temperatures T_d ~200 and 260 °C. The first minimum in the both curves corresponds to iron dehydration with CO and CO_2 evolution. Thus, at $T_d > 200$ °C a mobile medium is formed in which nucleation and growth of iron oxide clusters are possible. The second minimum is related, most likely, to the further removal of CO and CO_2 and the onset of agglomeration of the iron oxide clusters. The consistence between the thermodynamic model of cluster nucleation, growth, and agglomeration and the experimental data on iron oxalate thermal decomposition is illustrated in Fig. 3. Here the space isolated by dash includes four points of the onset of cluster nucleation and formation. The pre-critical region of cluster sizes ($r < r_{cr}$) corresponding to the stage of fluctuation nucleation accompanied by an increase in the $\Delta G(r)$ function is observed. In the region $r > r_{cr}$ the nucleation process is accompanied by a decrease in the free energy, occurs spontaneously, and is finished by the formation of a stable cluster with the size r_{max} = 5—6 nm and a nanosystem of weakly interacting clusters (see Fig. 3, *b*). Agglomeration occurs when the distance between the centers of adjacent clusters ($2r_t$) is rather short. In this case, if $r_{max} < r_t$, then in the region $r_{max} < r < r_t$ the $\Delta G(r)$ function increases to form a potential barrier with a maximum in the point $r = r_t$. With an increase in r_t the depth of the potential well corresponding to the strongly interacting system becomes smaller, and at $r_t = (r_t)_{max}$ the well disappears and agglomeration becomes impossible because it should be accompanied by an increase in the free energy ($\Delta G > 0$). Since r_{max} and r_t are determined by experimental conditions, the result of the topochemical reaction depends on the temperature of the reactor, duration of agglomera-

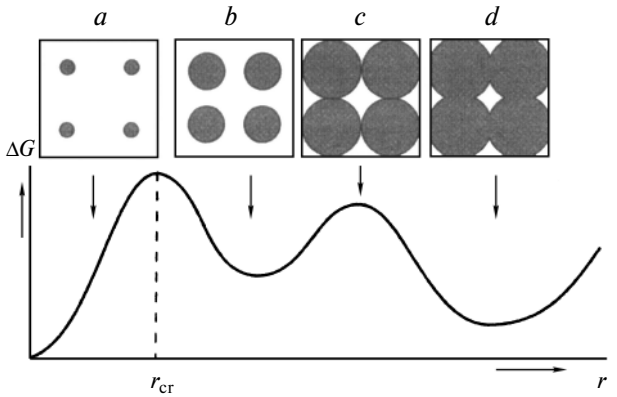

Fig. 3. Scheme of cluster formation, growth, and agglomeration: nucleation (*a*), maximum size of a stable cluster of a weakly interacting system (*b*), agglomeration onset (*c*), and formation of a system of strongly interacting clusters (*d*); arrows show the correspondence of stages *a*—*d* to the curve of changing the free Gibbs energy.

tion, and prehistory of the sample. Thus, the formation of a nanosystem proceeds *via* two main stages: the nanosystem of weakly interacting clusters (from the nucleation of clusters to the onset of their agglomeration) and the nanosystem of strongly agglomerating clusters (after the onset of their agglomeration). The change in the character of the intercluster interaction changes many properties of the nanosystem, and the appearance of the strong intercluster interaction and agglomeration is characterized by considerable interphase strains. These strains are generated by the formation of an intermediate neck due to surface tension[8]: $P = \alpha/x$, where α is the surface tension, and x is the neck radius for cluster agglomeration. Accepting for iron oxide $\alpha \approx 1$ N m^{-1} and $x \approx 1$ nm, we obtain $P \sim 10^9$ Pa. An excess pressure is also developed due to defects and dislocations at the interface and achieves 10^9 Pa for clusters ~10 nm in size.[1] The strain and pressure developed in the system of the strongly developed nanoclusters are important factors determining the formation of the nanostructure and its properties. When the conditions r_t and r_{max} are fulfilled, solid-phase nanoclusters of metals, oxides, and chalcogenides can be obtained, most likely, by low-temperature solid-phase reactions.

However, atomic nucleation followed by aggregation can be accompanied by cluster nucleation to form aggregates of individual clusters. In fact, when considering the change in the free energy G_{fa} of nucleation from individual clusters to form an aggregate with the R radius, as considered earlier for atoms (1), then

$$\Delta G_{fa} = 4\pi R^2\alpha_a - (4/3)\pi R^3\rho_a\Delta\mu_a, \quad (6)$$

where α_a, $\Delta\mu_a$, and ρ_a are the surface tension, the chemical potential of formation, and the density of the cluster aggregate, respectively.

Let N atoms, of which n_0 are iron atoms, fall per aggregate in a mixture, and $n_a = (4/3)\pi R^3\rho_a$ are those in the aggregate structure. Then for $N \gg n_0$

$$\Delta\mu_a = \Delta\mu_a{}^0 + \ln[(n_0 - n)/N]. \quad (7)$$

Here $\Delta\mu_a{}^0(PT)$ is the change in the standard chemical potential of iron measured in the kT units on going of one iron atom into the aggregate structure.

If cluster aggregates, similarly to individual clusters, do not contact with each other in the initial stage, then, designating the volume of this aggregate as $V_{fa} = (4/3)R^3$ and its surface as $S_{fa} = 4\pi R^2$, we can write Eq. (7) in the following form:

$$\Delta G_{fa} = \alpha_a S_{fa} - \{\Delta\mu_a{}^0 + \ln[(n_0 - n)/N]\}V_{fa}. \quad (8)$$

The ΔG_{fa} function, as for the atomic nucleation of an isolated cluster (see Fig. 1), has a maximum in the point $R = R_{cr}$ and a minimum in the point $R = R_{max}$. However, the r_{cr} and R_{cr} values should differ substantially.

In fact, the surface tension for a solid with a strong covalent bond between the iron and oxygen atoms on the surface of the iron oxide cluster should substantially exceed the surface tension for the cluster aggregates caused by weak van der Waals interactions between them. The surface tension values for these cluster aggregates are unknown; however, if accepting the surface tension for an iron oxide nanocluster to be about 1 N m^{-1} (Refs 9 and 10) and the surface tension of a cluster aggregate caused by hydrogen and van der Waals bonds to be, correspondingly, at a level between 0.073 N m^{-1} as for water and 0.02 N m^{-1} (Ref. 12) as for the most part of alkane molecules, then a 15—50-fold increase in the R_{cr} value for the cluster aggregate over r_{cr} can be expected from comparison of Eqs (3) and (8). Similar conclusion can be made from comparison of the energies of the bond between the iron and oxygen atoms in an iron oxide cluster (~2 eV for a covalent bond) and the energies of the bond between atoms of inert gases (~0.1 eV for a van der Waals bond); the latter is similar to the bond between the cluster aggregates.

The considered nucleation of the cluster aggregates can be not the single process of cluster aggregation. We can assume the existence of superaggregates including several cluster aggregates, whose formation occurs according to Eq. (8) but with lower surface tension and, hence, higher R_{cr} values.

Images and design of nanoclusters and nanostructures. Data of atomic force microscopy (AFM) and Mössbauer spectroscopy. The AFM images and profiles for the nanostructures of the iron oxide clusters obtained in the present work upon the thermal decomposition of iron(III) oxalate at $T_d = 210$ °C are shown in Fig. 4. The profiles of cross sections of the AFM image of the region 600×600 nm over lines *1* and *2* (see Fig. 4, *a*, *c*) indicate that two types of nanostructures are formed upon decomposition: larger aggregates 300 nm in size and smaller aggregates with sizes of 70—80 nm. Scanning of the region 300×300 nm (see Fig. 4, *b*, *d*) makes it possible to observe only one type of aggregates: 70—80 nm in size. The both scales of the images and especially the second one show the modulation of the profiles of the aggregates (roughness) with 25—35 particular peaks, indicating that the aggregates consist of finer parts: nanoclusters ~2—3 nm in size. However, the AFM method does not allow one to look inside a cluster aggregate to obtain the direct image of a nanocluster and determine its structure.

Mössbauer ^{57}Fe spectroscopy was used for this purpose. The Mössbauer spectra of the same nanostructure obtained at $T_d = 210$ °C are shown in Fig. 5. The magnetic HFS characteristic of γ-Fe_2O_3 is observed at the measurement temperature $T = 4.2$ K. This HFS was processed in the simplest model using two systems of magnetic HFS corresponding to atoms inside (1) and on the surface (2) of the cluster. As a result, we obtained the

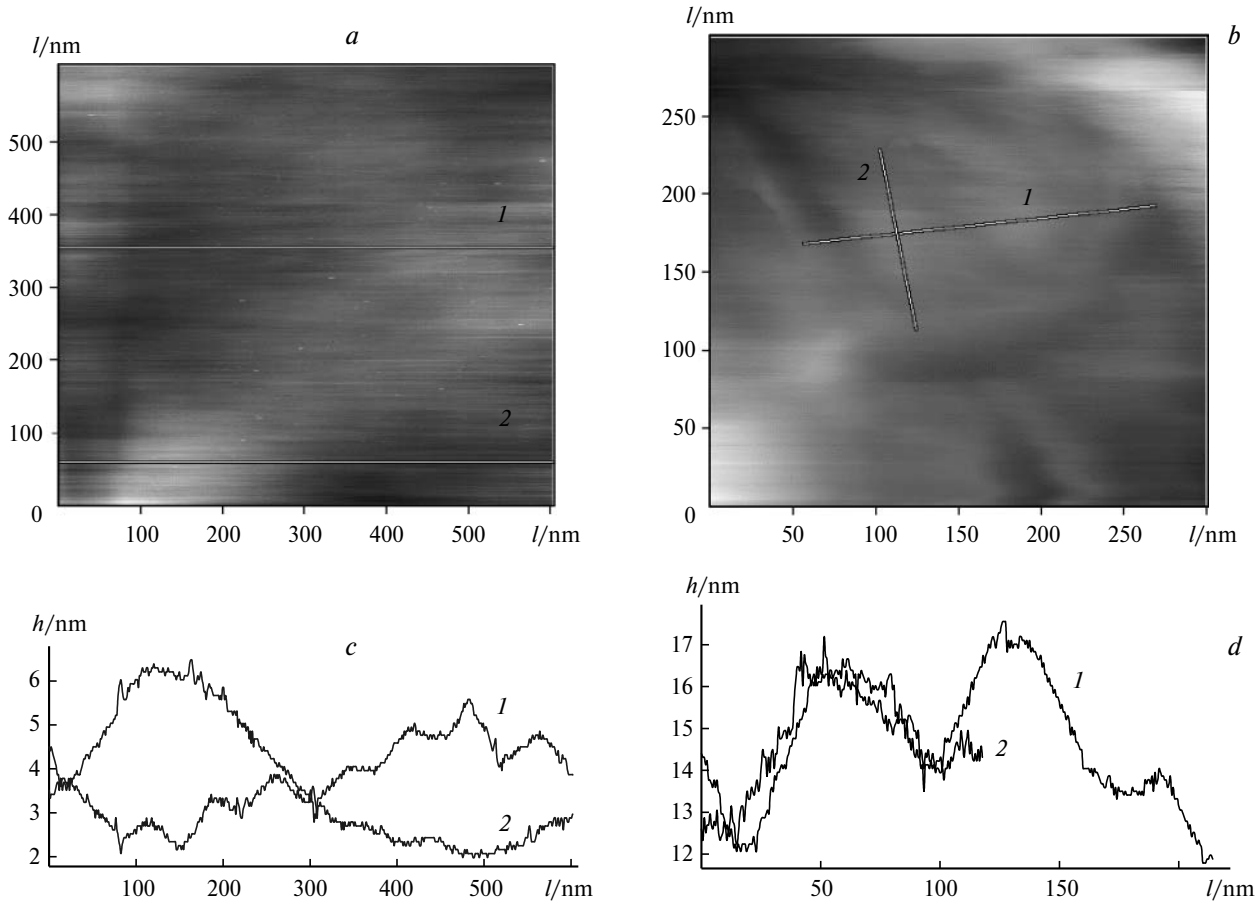

Fig. 4. AFM images (*a*, *b*) and the profiles of cross sections *1* and *2* of the AFM image (*c*, *d*) for the nanostructure including iron oxide nanoclusters and obtained at the decomposition temperature of iron oxalate T_d = 210 °C: 600×600 (*a*, *c*) and 300×300 (*b*, *d*).

values of the magnetic field on the nucleus $B_{in}(1)$ = 47.8±1.0 T and $B_{in}(2)$ = 42.8±1.0 T, isomeric shift $\delta(1)$ = 0.50±0.03 mm s^{-1} and $\delta(2)$ = 0.50±0.03 mm s^{-1}, and quadrupole splitting $\Delta(1) = \Delta(2) = 0$ mm s^{-1}. At this temperature the $B_{in}(1)$ value is somewhat lower than that for the bulk γ-Fe_2O_3 material (see Ref. 12), and their δ and Δ values coincide. The temperature increase results in diffusing of the spectrum, broadening of the magnetic HFS lines, and decreasing in B_{in}. Similar spectra are characteristic of superparamagnetic nanoclusters.

A phenomenon of superparamagnetism helps to estimate the nanocluster size. Let us use the simplest equation for superparamagnetism

$$\tau = \tau_0 \exp[KV/(kT)], \quad (9)$$

where τ, K, and V are the relaxation time of the magnetic moment, magnetic anisotropy constant, and cluster volume, respectively; $\tau_0 = 10^{-9}$—10^{-10} s. The relaxation time was estimated by the model of slow relaxation from broadening of the magnetic HFS lines.[13,14] For the spectra of the nanoclusters obtained at T_d = 210 °C, the line width (Γ) measured at T = 4.2 and 25 K was 0.62 and 5.12 mm s^{-1}, respectively. The value $\Delta\Gamma$ = 4.5 mm s^{-1} at T = 25 K corresponds to $\tau \approx 2.2 \cdot 10^{-9}$ s. Then for $\tau_0 = 10^{-9}$ at T = 25 K and $K = (1—2) \cdot 10^5$ J m^{-3} (see Ref. 15), the average cluster size is d = 1.4—1.7 nm. At the measurement temperature T = 78 K, the τ value decreases and only a quadrupole doublet with the parameters δ = 0.47±0.03 mm s^{-1} and Δ = 0.87±0.03 mm s^{-1} is observed in the Mössbauer spectrum.

The AFM data for larger clusters at T_d = 235 °C are presented in Fig. 6. Here no superaggregates including cluster aggregates are not already observed; however, cluster aggregates of approximately the same sizes as those for T_d = 210 °C (~80 nm) are retained. It is more difficult to see the cluster structure of these aggregates than those in the previous case; however, Mössbauer spectroscopy can help (Fig. 7). For the nanostructure obtained at T_d = 235 °C, the superparamagnetic transition is observed at a higher temperature (~100 K), which gives, using similar estimates, a cluster size of 4—7 nm.

The AFM images change drastically when the nanoclusters are transformed into the agglomeration state. Contact (touching) of adjacent clusters initiates the agglom-

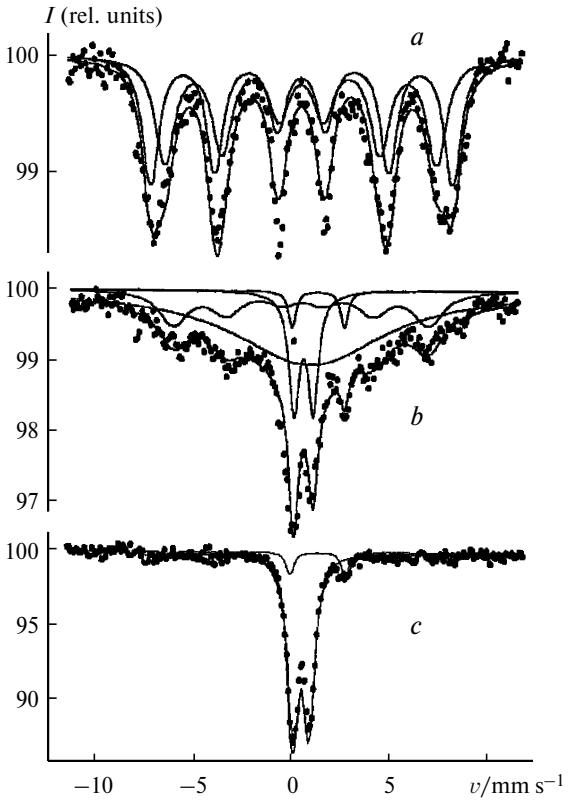

Fig. 5. Mössbauer spectra of the nanocluster including iron oxide nanoclusters and obtained at the decomposition temperature of iron oxalate T_d = 210 °C; recording temperature: 4.2 (*a*), 25 (*b*), and 78 K (*c*).

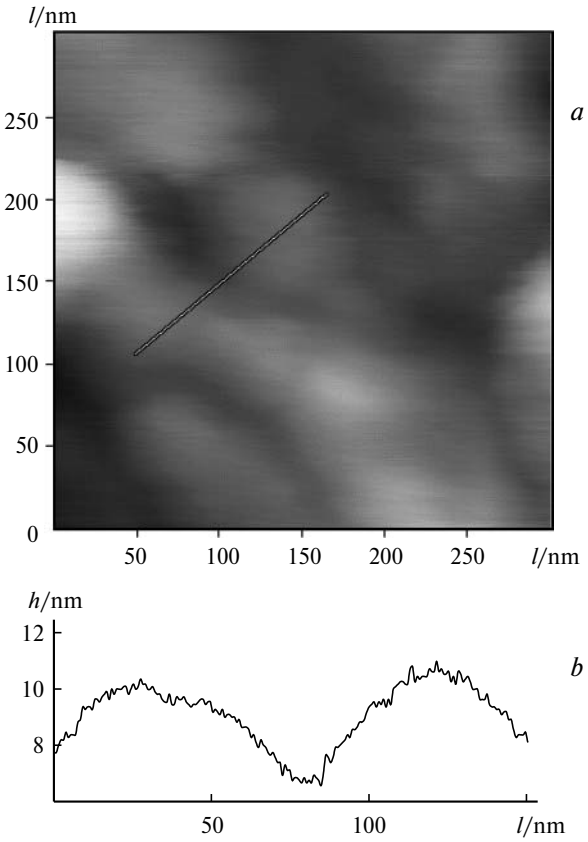

Fig. 6. AFM image (*a*) and the profile of the AFM image cross section (*b*) for the nanostructure including iron oxide nanoclusters and obtained at the decomposition of iron oxalate T_d = 235 °C.

eration process due to which a strongly interacting system is formed. The AFM images and profiles of the nanoclusters in the initial agglomeration stage at T_d = 265 °C are presented in Fig. 8. The study of the surface region 500×500 nm makes it possible to estimate a cluster size of 30—50 nm in a system of interacting clusters, and a larger scale (150×150 nm) and the study of the profile of two contacting nanoclusters give a half-width of 14 nm and a height of 6.4 nm for the prominent part of the cluster. The Mössbauer spectra of the nanocluster structure (Fig. 9) differ sharply from the spectra of the two preceding nanostructures considered. Despite the absence of superparamagnetic relaxation for these large clusters (calculations by formula (9) give the time values exceeding substantially the time characteristic of Mössbauer spectroscopy, $\tau \gg 10^{-8}$ s), a doublet characteristic of the paramagnetic or superparamagnetic state of the substance is observed in the spectrum up to T = 100 K. Processing of the Mössbauer spectra at T = 78 K results in two superfine magnetic structures corresponding to α-Fe_2O_3 with the parameters B_{in} = 52.0±1.0 T and Δ = −0.29±0.02 mm s^{-1} and to γ-Fe_2O_3 with the parameters B_{in} = 47.0±1.0 T and Δ = 0.00±0.02 mm s^{-1}. At T = 120 K and higher temperatures up to ambient temperature, the Mössbauer spectra can be presented by one system of the magnetic HFS and a quadrupole doublet with the parameters B_{in} = 51.3±1.0 T, Δ = 0.00±0.02 mm s^{-1}, δ = 0.45±0.02 mm s^{-1} and Δ = 0.78±0.02 mm s^{-1}, δ = 0.41±0.02 mm s^{-1}, respectively. The characteristic feature of the whole series of the Mössbauer spectra is the transformation of the spectra with the magnetic HFS into a quadrupole doublet corresponds, according to all the data, to the paramagnetic state of the substance at temperatures much lower than the Curie or Neel points typical of bulk α-Fe_2O_3 and γ-Fe_2O_3 (T_C = 965 K, T_N = 865 K). This result will be interpreted in the Section devoted to the magnetic properties of the nanostructures studied in the present work.

The AFM images for the largest nanoclusters obtained at T_d = 500 °C are shown in Fig. 10. Here we can see a nanostructure including strongly interacting nanoclusters in the agglomeration state with sizes of ~300 nm. The Mössbauer spectra of this system at room temperature correspond to bulk α-Fe_2O_3.[12]

Heat capacity of nanoclusters. The heat capacity of iron oxides is mainly caused by vibrations of atoms in the

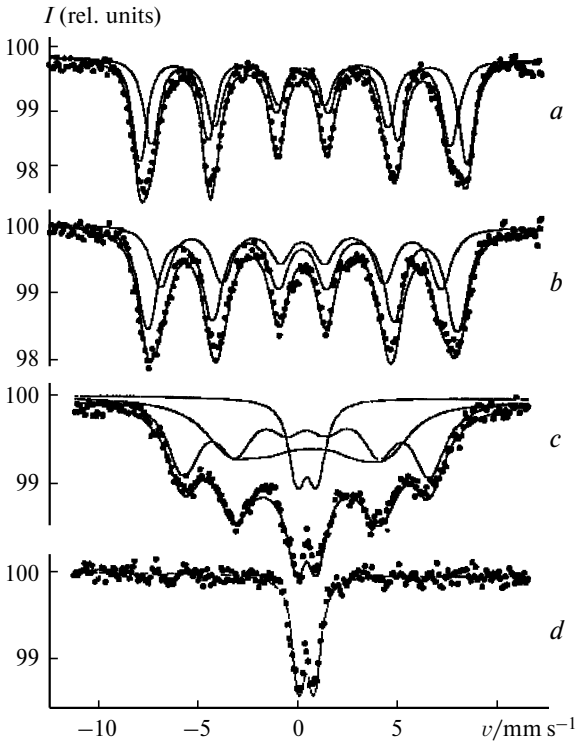

Fig. 7. Mössbauer spectra of the nanostructure including iron oxide nanoclusters and obtained at the decomposition temperature of iron oxalate T_d = 235 °C; recording temperature — 4.2 (*a*), 25 (*b*), 78 (*c*), and 110 K (*d*).

crystal lattice. For a crystal with finite sizes, the energy of atomic vibrations is written as follows:

$$E = (1/V)\sum_n h\omega_n/\{\exp[h\omega_n/(kT)] - 1\}, \qquad (10)$$

where summation is performed over $3N$ vibrational modes of the crystalline lattice including N atoms. The expression for heat capacity takes the form[16]

$$c = \frac{\partial E}{\partial T} = \frac{k}{V}\sum_n \left(\frac{h\omega_n}{kT}\right)^2 \frac{\exp[h\omega_n/(kT)]}{\{\exp[h\omega_n/(kT)] - 1\}^2}. \qquad (11)$$

The phonon frequencies ω_n depend on the shape and size of a crystal (cluster). In the asymptotic approximation for large spherical clusters with the R radii at high temperatures ($h\omega_n/k \ll T < T_C$, T_C is the critical temperature, for instance, Debye temperature), the heat capacity is expressed by the approximate formula[16]

$$c = c_B + aT^2/r + bT/r^2, \qquad (12)$$

where a and b are some constants. In the Debye approximation, this expression at $r \to \infty$ gives the formula

$$c = c_B = [kT^3/2\pi^2(ch)^3] \cdot p(T_C/T), \qquad (13)$$

where $p(x) = \int_0^x z^4 \exp z dz/(\exp z - 1)^2$, and c is the average sound speed.

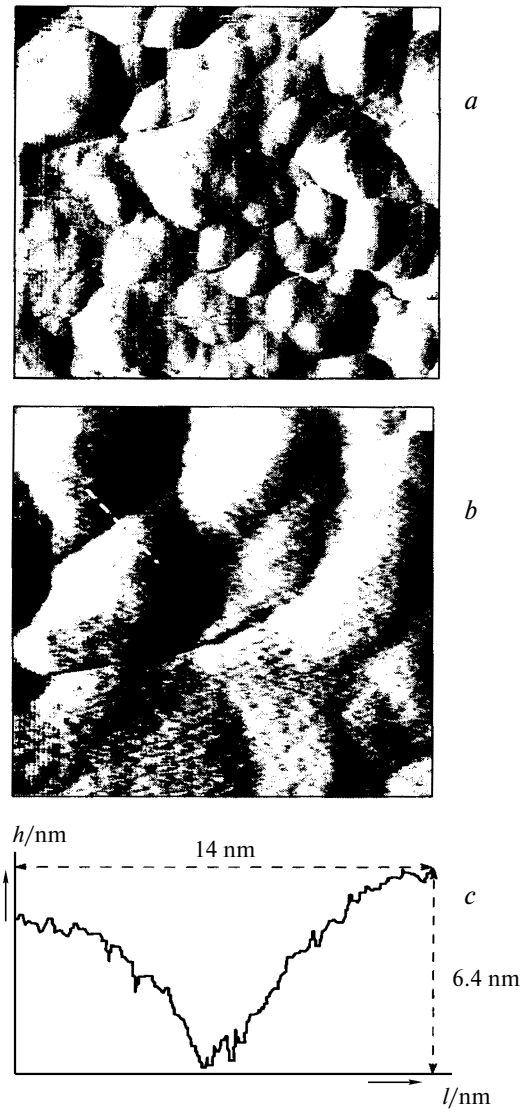

Fig. 8. AFM images of the nanostructure including iron oxide nanoclusters and obtained at the decomposition temperature of iron oxalate T_d = 265 °C: scanning regions 500×500 (*a*), 150×150 nm (*b*), and surface profile along the dashed line (see Fig. 8, *b*) (*c*); line length 14 nm, maximum depth of the relief 6.4 nm.

At high temperature ($T \gg T_d$) this expression leads to the Dulong—Petit law

$$c = 3R \qquad (14)$$

(R is the universal gas constant), and at low temperatures ($T \ll T_d$, $T < 0.1T$) we obtain the expression

$$c = a(T/T_d)^3. \qquad (15)$$

The low-temperature limit at $T \to 0$ gives the approximation in the form

$$c \approx (1/V)[(h\omega_0)^2/(kT)^2]\exp[-(h\omega_0)/(kT)], \qquad (16)$$

where ω_0 is the minimum phonon frequency.

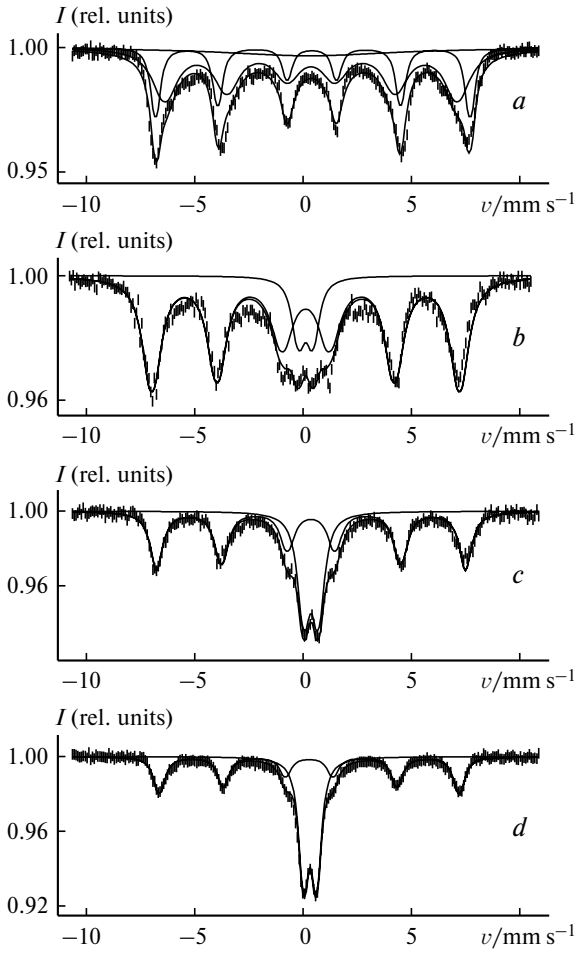

Fig. 9. Mössbauer spectra of the nanostructure including iron oxide nanoclusters and obtained at the decomposition temperature of iron oxalate T_d = 265 °C; recording temperature 77.8 (*a*), 125 (*b*), 160 (*c*), and 300 K (*d*).

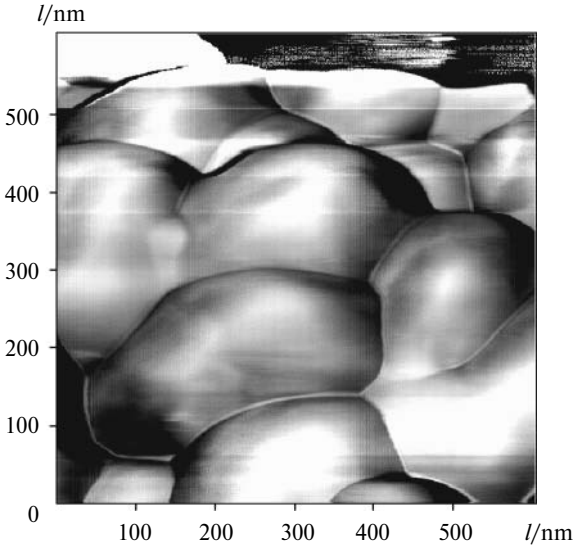

Fig. 10. AFM image of the nanostructure including iron oxide nanoclusters and obtained at the decomposition temperature of iron oxalate T_d = 500 °C.

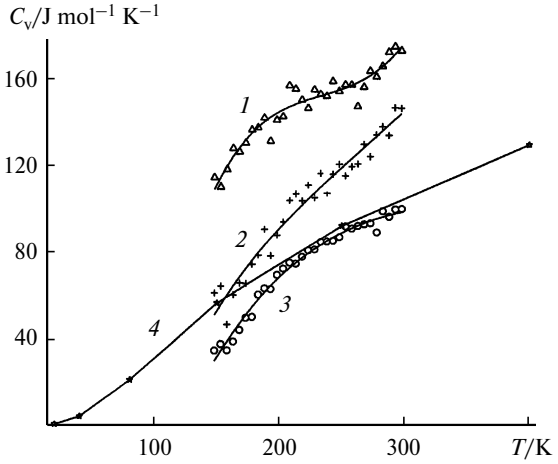

Fig. 11. Molar heat capacity for nanostructures including iron oxide nanoclusters with average sizes 2—3 (*1*), 4—7 (*2*), and 300 nm (*3*) and bulk iron oxide (*4*).

Analysis of Eqs (10)—(16) suggests that the heat capacity of the nanoclusters should increase compared to that of a bulk solid in a wide temperature range, and the increase in the heat capacity $\Delta = c - c_B$ for the nanoclusters is due to an increase in the specific surface and the appearance of additional modes of atomic vibrations ($\sim aT^2/r$) and to a possible restriction of the wavelength of phonons ($\sim bT/r^2$) due to a decrease in the linear size of the cluster. Consideration of the low-temperature limit (16) makes it possible to predict a decrease in the heat capacity of the nanoclusters compared to that of a bulk solid ($\Delta = c - c_B < 0$), so that for some size the heat capacity of the nanoclusters becomes equal to that of a bulk substance and then decreases with the further temperature decrease.

The temperature plots of the heat capacity of the system of weakly interacting nanoclusters with sizes from 2—3 nm to 300 nm are shown in Fig. 11. A similar temperature dependence of a bulk iron oxide sample is presented for comparison. A considerable increase in the heat capacity of the nanoclusters over that of the bulk material is distinctly seen and for the nanoclusters with the sizes 2—3 nm exceeds that for the bulk sample by almost 2 times. The second distinctive feature of the heat capacity of the nanoclusters compared to the bulk solid is a great slope of the temperature dependence of the heat capacity for the nanoclusters.

Let us consider reasons for an increase in the heat capacity according to Eqs (13)—(16). The first reason is related to an increase in the root-mean-square displacements of atoms on the solid surface $\langle x \rangle^2$ compared to atoms inside the substance due to a decrease in the num-

ber of bonds on the surface over that in the bulk. This increases the $\langle x \rangle^2$ values for atoms on the surface by 2 times.

However, this increase is expected only for atoms on the isolated solid surface or on the surface of isolated clusters. Any interaction with the surface or intercluster interaction induces an increase in the number of bonds and a decrease in $\langle x \rangle^2$. The heat capacity is not directly related to the $\langle x \rangle^2$ values and, therefore, its double increase can hardly be explained by the simple increase in $\langle x \rangle^2$. Indeed, when taking the simplest expression for this magnitude in the Debye high-temperature approximation, then

$$\langle x \rangle^2 \cong kT/(M\omega^2), \quad (17)$$

where M is the mass of the atom.

It can easily be obtained that if in the harmonic approximation the energy of oscillator vibrations can be presented in the form

$$E \cong \varepsilon \langle x \rangle^2 \quad (18)$$

(ε is the elasticity constant), then

$$c \cong \varepsilon k/(M\omega^2). \quad (19)$$

Analysis of this expression shows a strong effect of the frequency spectrum of the nanocluster on the heat capacity. The appearance of low-temperature vibrations (and the corresponding increase in $\langle x \rangle^2$) in the phonon spectrum of the cluster results in a considerable increase in the heat capacity. At the same time, as already mentioned, a decrease in the cluster size can be accompanied by the restriction of the phonon wavelength and the frequency cut of the phonon spectrum from the low-frequency side, which can induce a decrease in the heat capacity.

The second constant determining the heat capacity of the nanoclusters is the elasticity constant of atomic vibrations in the cluster. For instance, a change in the state of the nanosystem with the temperature increase and its transformation into, *e.g.*, the liquid state changes this constant. Therefore, the heat capacity of the substance upon its transformation into the liquid state can be either higher or lower than the heat capacity of the initial state. It is difficult to unambiguously conclude about an increase in the heat capacity with a decrease in the cluster size based on analysis of changes in $\langle x \rangle^2$, the frequency spectrum, and elastic constants.

At the same time, a study[17] of the intracluster mobility of iron atoms in the iron oxide clusters at room temperature showed that the clusters 1—5 nm in size possess an enhanced atomic mobility, and the atomic dynamics of the clusters 1—2 nm in size is very sensitive to the state of the cluster surface, effect of the surface tension, and influence of surfactants. A parameter was proposed for such a special dynamic state of the nanocluster: the critical size of the cluster. When the size of the cluster is smaller than this critical size, the cluster is transformed into a solid—liquid state like slush (see, *e.g.*, Ref. 18). Thus, according to this interpretation, the iron oxide clusters with sizes of 1—2 nm are characterized by a decrease in the melting point down to ambient temperature and transformation into a special solid—liquid state. This state explains such a high heat capacity value for the iron oxide nanoclusters.

In fact, the heat capacity of many solids can decrease or increase after melting. However, near the melting point corresponding to the phase transition, *viz.*, melting, the heat capacity increases considerably (sometimes even by several times).[11] This behavior of the heat capacity during phase transition allows one to explain the considerable increase in the heat capacity of small clusters near ambient temperature along with the frequency change in the phonon spectrum and an increase in the $\langle x \rangle^2$ value.

The second feature of the temperature behavior of the heat capacity of the iron oxide nanoclusters is related to a sharper temperature dependence at $T < 200$ K compared to the bulk material. A similar temperature dependence was observed for nanoclusters of metals, for instance, silver,[19] when at some temperature the heat capacity values of the cluster cross the temperature plot of the heat capacity for the bulk material and become lower than those for the bulk material. For metals, a similar effect can easily be explained by the effect of quantum restraint of phonons in the cluster and the influence of the linear term including (at low temperatures) the $1/r^2$ values as well. Analogous data for the metal oxide clusters are missing, and the results obtained at relatively high temperatures can be attributed, most likely, to the effect of a complicated structure of the oxide cluster, the presence of atoms of another type (oxygen), the influence of defects favoring the appearance of high-frequency optical vibrations, and a possible low-frequency "cut" of the phonon spectrum.

Magnetic properties of nanoclusters and nanostructures. Isolated and weakly interacting nanoclusters obtained in solid-phase chemical reactions (see above) and in polymeric or other non-magnetic matrices are superparamagnetic. This is related to the fact that the total magnetic moment of a nanocluster is confirmed by thermal fluctuations as a single whole without loss of magnetic ordering between particular magnetic atoms. The fluctuation time of the magnetic moment is described by formula (9).

According to the Mössbauer spectroscopic data, these values are $2.2 \cdot 10^{-9}$ s for the iron oxide nanoclusters 1—2 nm in size at $T = 25$ K (see Fig. 5). An increase in the cluster size results in an elongation of the fluctuation time. This causes, in turn, the dependence of the superparamagnetic properties on the measurement methods. For instance, for Mössbauer spectroscopy at fluctuation

times more than the characteristic time of the method ($\tau > 10^{-8}$ s), the magnetic HFS of the spectrum related to magnetic ordering of the nanocluster appears. For measuring magnetization, for example, using a SQUID magnetometer with the characteristic times 1—10 s, at $\tau < 1$—10 s magnetic clusters of similar size will be superparamagnetic.

In the case of the nanoclusters with the fluctuation time more than the characteristic time of the method, the temperature dependence of the magnetization can be observed considering the mean magnetization M_C of the nanoclusters with magnetic moments arbitrarily oriented in the space[20]:

$$M_C = M_S \frac{\int \exp[-E(\theta)/(kT)] \cos\theta \sin\theta d\theta}{\int \exp[-E(\theta)/(kT)] \sin\theta d\theta}, \quad (20)$$

where M_S is the saturation magnetization, and θ is the angle between the magnetization direction and easy axis of cluster magnetization. If the effect of magnetic anisotropy is negligible compared to the magnetic field effect, then Eq. (20) can be written in a simpler form

$$M_C = M_S L[mH/(kT)], \quad (21)$$

where $m = M_S V$ is the magnetic moment of the cluster, and

$$L[mH/(kT)] = \coth[mH/(kT)] - kT/(mH) \quad (22)$$

represents the Langevin function, which at $mH \ll kT$ results in the magnetization of a superparamagnetic, which is similar to the expression for the Curie law for paramagnetics

$$M_C = M_S^2 VH/(3kT). \quad (23)$$

A similar temperature dependence of the magnetization was observed for the weakly interacting iron oxide nanoclusters with sizes of 1—2 nm (Fig. 12, curves *1* and *1′*) up to 50 K. The results of measuring the magnetization on cooling of the sample in the magnetic field (*1*) and in the absence of a field (*1′*) are presented in Fig. 12. This procedure is one of the main methods of studying the effect of superparamagnetism on the magnetization of the sample. In the case of superparamagnetism, two types of dependences are observed[21]: cooling in the magnetic field results in a smooth hyperbolic dependence of the sample magnetization of the type $1/T$, and cooling in the absence of a magnetic field also results in a similar dependence but only to the temperature T_B, *i.e.*, to the temperature at which thermal fluctuations of the magnetic moment of the cluster cease. Below this temperature the magnetization decreases to zero, because the resulting magnetic moment of the whole nanosystem tends to zero due to the chaotic direction of the magnetic moment of each nanocluster.

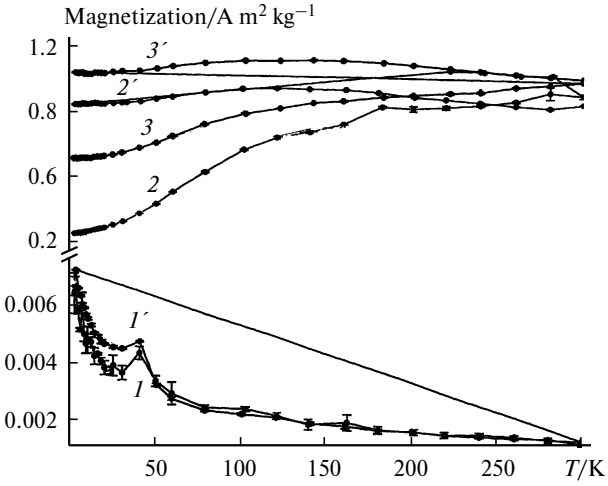

Fig. 12. Magnetization of nanostructures obtained at the decomposition temperature of iron oxalate T_d = 210 (*1*, *1′*), 265 (*2*, *2′*), and 330 °C (*3*, *3′*) and including iron oxide nanoclusters with the average sizes 2—3 nm (*1*, *1′*), 30—50 nm (*2*, *2′*), and larger (*3*, *3′*). Magnetization was measured after cooling the samples in the presence of an external magnetic field of 10 Oe (*1—3*) and in the absence of the field (*1′—3′*).

The run of the magnetization curves in the range T = 4.2—50 K for the system of weakly interacting iron oxide nanoclusters (see Fig. 12, curve *1*) differs significantly from the standard pattern of superparamagnetism. At $T \approx 40$ K the magnetization maximum is observed, which is accompanied by a small descent and then an ascent with the temperature decrease to 4.2 K not only for the field dependence but also for the samples upon their cooling in the absence of a magnetic field. This contradicts the superparamagnetic behavior of isolated or weakly interacting clusters. To explain this effect, it is necessary to consider again nanocluster design for a system of the weakly interacting iron oxide clusters (see Fig. 4). An hierarchic structure was observed for this system: the primary nanoclusters 1—2 nm in size enter into the composition of a more complicated structural agglomerate 70—80 nm in size. The formation of such an aggregate is determined by the surface tension and a decrease in the free energy, which should inevitably be accompanied by approaching and intercluster ordering of the primary iron oxide clusters. This aggregate can be considered as a molecular magnet formed of individual molecules, *viz.*, primary iron oxide clusters, and transforming into the magnetically ordered state in the Curie (Neel) point at 30—40 K due to exchange interactions between the primary clusters. Thus, below T_B ~50 K the magnetic phase transition occurs in the range T = 30—40 K to form the magnetically ordered cluster structure of the cluster aggregate.

The results of studying the magnetization of the nanostructure including the weakly interacting super-

paramagnetic clusters (see Fig. 12, curves *1* and *1′*) make it possible to develop a model of magnetic ordering of magnetic moments of individual iron atoms in the composition of the primary cluster. In fact, a maximum magnetization value of $\sim 10^{-2}$ A m^2 kg^{-1} results in the ultimately low value of the magnetic moment of the cluster (~0.1 μ_B per cluster) compared to the magnetic moment of the Fe^{3+} ion (5—6 μ_B). This type of magnetic ordering is observed for very small clusters with the very large specific surface and is named speromagnetic ordering.[22] A similar type of ordering can be presented schematically as a fan-shaped arrangement of magnetic moments of individual atoms directed from the cluster center to its periphery with a uniform change in the magnetic moment direction from 0 to 180° relatively to any distinguished direction. The total magnetic moment corresponds to the incomplete compensation of particular magnetic moments of atoms for this type of magnetic ordering in the cluster.

Quite different magnetic ordering and magnetic structures are characteristic of nanosystems with the strong intercluster interaction, which results in the temperature dependences of the magnetization (see Fig. 12, curves *2*, *2′* and *3*, *3′*). These data correspond to a magnetically ordered nanostructure without superparamagnetism properties. The high-temperature (200—300 K) and low-temperature (4.2—200 K) intervals of magnetization measurements can be considered.

The high-temperature interval is characterized by the almost complete absence of both temperature and dimensional effects. The external magnetic field effect, which is used to change the state of the sample during its cooling, is virtually absent. When comparing these results with the data of Mössbauer spectroscopy (see Fig. 9) according to which the non-magnetic (paramagnetic) component is observed in the spectrum down to 100 K, it becomes evident that this spectrum does not correspond to the appearance of superparamagnetism in the nanostructures 30—50 nm in size (see Fig. 12, curves *2* and *2′*) and, the more so, in larger clusters (see Fig. 12, curves *3* and *3′*). The appearance of the quadrupole paramagnetic doublet in the Mössbauer spectra is due to the first-order phase transition in this system, when the magnetization of the nanocluster disappears jumpwise after some critical temperature (analog of the Curie or Neel temperature for a bulk solid) or a critical size (at a smaller size the cluster looses magnetization jumpwise and is transformed into the paramagnetic state omitting the superparamagnetic stage) is achieved.[23—25] The appearance of such a transition in the relatively large iron oxide nanoclusters with sizes of several tens of nanometers is due to the influence of defects in the nanostructure. The optimal range of cluster sizes corresponds to the appearance of the greatest defect concentration, because for the large nanoclusters the defect density is low due to a low specific surface, whereas for small nanoclusters the surface tension of the cluster "pull out" all intracluster defects onto the surface, and the concentration of defects passes through the maximum and begins to decrease with a decrease in the cluster size.[26] No substantial changes in the magnetization of the samples were observed in the high-temperature interval, evidently, due to their magnetic saturation in the magnetic field of the magnetometer during temperature measurements.

There is one more important characteristic of the α-Fe_2O_3—γ-Fe_2O_3 nanoclusters: the formation of a twinned structure. According to the data of Mössbauer spectroscopy (see Fig. 9), above T = 120 K their nanostructure is characterized by averaged parameters of the magnetic HFS corresponding to twin formation, which is initiated by the Morin phase transition in the α-Fe_2O_3 nanoclusters.[27] This transition is a jumpwise change in the directions of magnetic moments by 90° and the transformation of the high-temperature non-compensated antiferromagnetic (weak ferromagnetic) into the low-temperature compensated antiferromagnetic. Twinned structures are also known for a series of the nanoclusters with two crystalline modifications for the bulk material, for instance, Zr_2O_3.[28] The bulk α-Fe_2O_3 sample is known to possess the Morin transition at T = 250 K, when the high-temperature crystalline modification providing weak ferromagnetism is transformed into the low-temperature modification corresponding to compensated antiferromagnetism.

The low-temperature region of magnetization of the α-Fe_2O_3—γ-Fe_2O_3 nanostructure below T = 200 K is characterized by a considerable decrease in the magnetization with the temperature decrease and the presence of a dependence of the nanocluster size and the method of sample cooling (in the magnetic field or without a field) (see Fig. 12, curves *2*, *2′* and *3*, *3′*). The decrease in the magnetization of the α-Fe_2O_3—γ-Fe_2O_3 nanostructure is attributed to the transformation of the twinned structure into the α-Fe_2O_3—γ-Fe_2O_3 nanostructure to form the antiferromagnetic compound α-Fe_2O_3. In this case, the magnetization value of 0.2 A m^2 kg^{-1} corresponds to the γ-Fe_2O_3 nanoclusters. The distributed transition to the state corresponding to compensated antiferromagnetism at T < 200 K is related to the size distribution of clusters. In fact, above the Morin point bulk α-Fe_2O_3 possesses non-compensated antiferromagnetism, and the deviation of the magnetic moment directions of adjacent iron atoms in the crystal cell corresponds to

$$\alpha \approx E_M/E_{Ex}, \qquad (24)$$

where E_M is the magnetic dipole energy, and E_{Ex} is the exchange energy.

This ratio and, correspondingly, the angle of turn (non-compensation of the magnetic moments) is 10^{-2}—10^{-5}, and for bulk α-Fe_2O_3 this value is ~10^{-3} (see Ref. 29). For

the nanoclusters, the α value should increase with an increase in the specific surface and a decrease in the exchange energy, which results in a decrease in T_M with a decrease in the cluster size. For nanocluster sizes of several nanometers, the Morin transition is absent and the nanostructure is not transformed into the state of compensated antiferromagnetism.

Cooling of the samples in the magnetic field H = 10 Oe should result in the enlargement of the temperature region where weak antiferromagnetism exists according to the expression

$$\alpha \approx E_M + mH/E_{Ex} \quad (25)$$

(m is the magnetic moment of the cluster), which leads to a considerable increase in the magnetization to 1 A m^2 kg^{-1} at T = 4.2 K.

The larger α-Fe_2O_3—γ-Fe_2O_3 nanoclusters (corresponding to the higher decomposition temperature of the primary iron salt) (see Fig. 12, curves *3* and *3′*) demonstrate a similar effect with the great contribution of magnetization of the γ-Fe_2O_3 nanoclusters with the ferrimagnetic spinel structure. Thus, at low temperatures the magnetization of the α-Fe_2O_3—γ-Fe_2O_3 nanostructure on cooling in the absence of a magnetic field is determined by the magnetization of the ferrimagnetic γ-Fe_2O_3 nanoclusters. Cooling in the magnetic field results in magnetic saturation of the samples and a weak temperature dependence in both the high- and low-temperature regions.

Thus, different types of the nanostructures were synthesized in the present work on the basis of the iron oxide clusters with sizes from ~1 to ~300 nm, including the nanosystems with weak and strong intercluster interactions. The nanostructures with the weak intercluster interactions consist of cluster aggregates 70—80 nm in size that are incorporated into larger superaggregates with a size of ~300 nm and including, in turn, primary atomic clusters of iron oxide 2—3 nm in size. The nanoclusters with the strong intercluster interaction have no hierarchic structure and represent a nanosystem of agglomerating clusters with the sizes from 30 to 300 nm. The heat capacity of the iron oxide nanoclusters 2—3 nm in size is by 2 times higher than that for the bulk material. This is caused by a change in the phonon spectrum (increase in the specific surface) and a possible transition of these nanoclusters to a special solid—liquid state. The magnetic properties of these α-Fe_2O_3—γ-Fe_2O_3 nanostructures vary from superparamagnetic to magnetically ordered with an increase in the nanocluster size from 2—3 to 30—50 nm. For the aggregate nanostructure, the phase transition to the magnetically ordered state was found near T = 50 K when the cluster aggregate acts as some molecular magnet, where the primary clusters 2—3 nm in size play the role of molecules. A twinned structure is observed for the magnetically ordered α-Fe_2O_3—γ-Fe_2O_3 nanostructures at temperatures above 120 K, and magnetic phase transitions of the first order are observed at temperatures above 100 K, when magnetic ordering in the nanosystem disappears jumpwise at some temperature lower than T_C or T_N for the bulk material or with the particle decrease after some critical size of 30—40 nm when the nanosystem is transformed into the superparamagnetic state.

This work was financially supported by the Russian Foundation for Basic Research (Project Nos 06-03-32006 and 06-03-33052).

References

1. D. W. Oxtoby, *Advances in Chemical Physics*, J. Wiley, New York, 1988, 263.
2. I. P. Suzdalev and P. I. Suzdalev, *Usp. Khim.*, 2001, **70**, 203 [*Russ. Chem. Rev.*, 2001, **70**, 177 (Engl. Transl.)].
3. I. P. Suzdalev, Yu. V. Maksimov, V. N. Buravtsev, V. K. Imshennik, A. G. Kazakevich, and S. V. Novichikhin, *Kolloid. Zh.*, 2000, **62**, 257 [*Colloid J.*, 2000, **62**, 224 (Engl. Transl.)].
4. I. P. Suzdalev, V. N. Buravtsev, V. K. Imshennik, and S. V. Novichikhin, *Khim. Fiz.*, 1993, **12**, 555 [*Chem. Phys. Reports*, 1993, **12**, 501 (Engl. Transl.)].
5. I. P. Suzdalev, *Zh. Obshch. Khim.*, 2002, **72**, 591 [*Russ. J. Gen. Chem.*, 2002, **72** (Engl. Transl.)].
6. A. I. Gusev and A. A. Rempel´, *Nanokristallicheskie materialy* [*Nanocrystalline Materials*], Fizmatlit, Moscow, 2000 (in Russian).
7. I. P. Suzdalev, *Dinamicheskie effekty v gamma-rezonanasnoi spektroskopii* [*Dynamic Effects in γ-Resonance Spectroscopy*], Atomizdat, Moscow, 1979, p. 51 (in Russian).
8. Ya. G. Geguzin, *Fizika spekaniya* [*Physics of Agglomeration*], Nauka, Moscow, 1984, 70 (in Russian).
9. W. D. Kingery, H. K. Bowen, and D. R. Ulmann, *Introduction to Ceramics*, J. Wiley, New York, 1976, 183.
10. B. F. Ormont, *Dokl. Akad. Nauk SSSR*, 1959, **124**, 132 [*Dokl. Chem.*, 1959 (Engl. Transl.)].
11. *Fizicheskie velichiny. Spravochnik* [*Physical Magnitudes. Reference Book*], Eds I. R. Grigor´ev and U. S. Meilikhov, Energoatomizdat, Moscow, 1991, 1232 pp. (in Russian).
12. *Chemical Applications of Mossbauer Spectroscopy*, Eds V. I. Goldanskii and R. H. Herber, Academic Press, New York—London, 1968.
13. I. P. Suzdalev, A. M. Afanas´ev, A. S. Plachinda, V. I. Gol´danskii, and E. F. Makarov, *Zh. Eksp. Teor. Fiz.*, 1974, **55**, 1752 [*J. Exp. Theor. Phys.*, 1974, **55** (Engl. Transl.)].
14. I. P. Suzdalev, I. V. Kurinov, E. Yu. Tsymbal, and V. V. Matveev, *J. Phys. Chem. Sol.*, 1994, **55**, 127.
15. J. M. D. Coey and D. Khalafalla, *Phys. Status. Sol.*, 1972, **11**, 2290.
16. Th. F. Nonnenmacher, *Phys. Lett.*, 1975, **51A**, 213.
17. I. P. Suzdalev and N. I. Shklovskaya, *Colloid Surf. A*, 1996, **108**, 315.
18. R. S. Berry, in *Clusters of Atoms and Molecules*, Ed. H. Haberland, Springer-Verlag, Berlin, 1994, 201.
19. G. Goll and H. Lohneyen, *Nanostruct. Mater.*, 1995, **6**, 559.

20. S. Morup, *Paramagnetic and Superparamagnetic Relaxation Phenomena Studied by Mossbauer Spectroscopy*, Polyteknisk Forlag, Lyngby, 1981, 191.
21. D. L. Leslie-Pelesky and R. D. Rieke, *Chem. Mat.*, 1996, **8**, 1770.
22. J. M. D. Coey, *J. Phys.*, 1974, **35**, C6-83.
23. I. P. Suzdalev, *Fiz. Tverd. Tela*, 1970, **12**, 988 [*Sov. Phys.-Sol. St.*, 1970, **12**, 775 (Engl. Transl.)].
24. I. P. Suzdalev, V. N. Buravtsev, V. K. Imshennik, Yu. V. Maksimov, S. V. Novichikhin, A. X. Trauwein, and H. Winkler, *Z. Phys. D*, 1996, **37**, 55.
25. I. P. Suzdalev, V. N. Buravtsev, V. K. Imshennik, and Yu. V. Maksimov, *Scripta Mater.*, 2001, **44**, 1937.
26. I. P. Suzdalev, V. N. Buravtsev, Yu. V. Maksimov, A. A. Zharov, V. K. Imshennik, S. V. Novichikhin, and V. V. Matveev, *Izv. Akad. Nauk*, *Ser. Khim.*, 2003, 1848 [*Russ. Chem. Bull., Int. Ed.*, 2003, **52**, 1950].
27. I. P. Suzdalev, Yu. V. Maksimov, S. V. Novichikhin, V. N. Buravtsev, V. K. Imshennik, and V. V. Matveev, *Khim. Fiz.*, 2000, **19**, 105 [*Chem. Phys. Reports*, 2000, **19**, 401 (Engl. Transl.)].
28. V. Ya. Shevchenko, *Problemy i dostizheniya fiziko-khimicheskoi i inzhenernoi nauki v oblasti nanomaterialov* [*Problems and Achievements of Physicochemical and Engineering Science in the Field of Nanomaterials*], Ed. V. A. Makhlin, L. Ya. Karpov Physicochemical Research Institute, Moscow, **2**, 185 (in Russian).
29. S. V. Vonsovskii, *Magnetizm* [*Magnetism*], Nauka, Moscow, 1971, 1024 pp. (in Russian).

Received February 7, 2006;
in revised form March 14, 2006